Distinct Functional Interactions between Actin Isoforms and Nonsarcomeric Myosins

Mirco Müller[1], Ralph P. Diensthuber[1¤a], Igor Chizhov[1], Peter Claus[2], Sarah M. Heissler[1¤b], Matthias Preller[1], Manuel H. Taft[1], Dietmar J. Manstein[1]*

1 Institute for Biophysical Chemistry, Hannover Medical School, Hannover, Germany, 2 Institute of Neuroanatomy, Hannover Medical School, Hannover, Germany

Abstract

Despite their near sequence identity, actin isoforms cannot completely replace each other *in vivo* and show marked differences in their tissue-specific and subcellular localization. Little is known about isoform-specific differences in their interactions with myosin motors and other actin-binding proteins. Mammalian cytoplasmic β- and γ-actin interact with nonsarcomeric conventional myosins such as the members of the nonmuscle myosin-2 family and myosin-7A. These interactions support a wide range of cellular processes including cytokinesis, maintenance of cell polarity, cell adhesion, migration, and mechano-electrical transduction. To elucidate differences in the ability of isoactins to bind and stimulate the enzymatic activity of individual myosin isoforms, we characterized the interactions of human skeletal muscle α-actin, cytoplasmic β-actin, and cytoplasmic γ-actin with human myosin-7A and nonmuscle myosins-2A, -2B and -2C1. In the case of nonmuscle myosins-2A and -2B, the interaction with either cytoplasmic actin isoform results in 4-fold greater stimulation of myosin ATPase activity than was observed in the presence of α-skeletal muscle actin. Nonmuscle myosin-2C1 is most potently activated by β-actin and myosin-7A by γ-actin. Our results indicate that β- and γ-actin isoforms contribute to the modulation of nonmuscle myosin-2 and myosin-7A activity and thereby to the spatial and temporal regulation of cytoskeletal dynamics. FRET-based analyses show efficient copolymerization abilities for the actin isoforms *in vitro*. Experiments with hybrid actin filaments show that the extent of actomyosin coupling efficiency can be regulated by the isoform composition of actin filaments.

Introduction

Mammalian actin isoforms are highly conserved and ubiquitously found in eukaryotic cells. The 42 kDa globular actin monomer is composed of four subdomains and can assemble into thin filaments or microfilaments (F-actin). Six actin isoforms can be distinguished: three α-actin isoforms (α-skeletal muscle, α-cardiac muscle and α-vascular), one β-isoform (β-cytoplasmic) and two γ-isoforms (γ-cytoplasmic and γ-smooth muscle). Only subtle sequence variations distinguish the isoactins. The amino acid sequence of α-actin differs from cytoplasmic actin isoforms in more than 20 residues that are spread over the entire molecule. In contrast, differences between β- and γ-actin are restricted to the N-terminus – Asp^2-Asp^3-Asp^4-Ile^5 (β-actin) and Glu^2-Glu^3-Glu^4-Ile^5 (γ-actin). The N-terminal sequences of α-skeletal and α-cardiac actin correspond to Asp^3-Glu^4-Asp^5-Glu^6 and Asp^3-Asp^4-Glu^5-Glu^6 [1]. Actin isoforms are essential for a wide range of physiological functions. The four muscle actins are restricted to tissues with high tonic activity such as striated heart muscle, skeletal muscle or smooth muscle of blood vessels, gut wall and the urogenital system [2]. By contrast, cytoplasmic actins are ubiquitous and play a pivotal role in cell motility, intracellular transport, cell shape maintenance or mitosis [3]. They undergo spatial and temporal segregation during the formation of stress fibers and actin-based cell protrusions [4,5]. The resulting structures are regulated by specific actin-binding proteins [6,7]. There is strong evidence that the isoactins cannot substitute for each other [8,9,10,11], indicating functional intracellular specialization [12,13]. The β-isoform preferably localizes in stress fibres, circular bundles and at cell-cell contacts as an unbranched filamentous array. Dependent on cellular activities, γ-actin displays a more variable distribution. It is mainly organized as a branched meshwork with cortical and lamellar localization in moving cells, but can colocalize with β-actin in lamellipodia or be recruited into stress fibres [3,12]. Knockout studies in mice revealed, that both cytoplasmic actin isoforms are required for stereocilia maintenance in hair cells [14]. Aberrant expression of particular isoactins is a significant feature of adaptive and pathological alterations in e.g. wound healing, cardiovascular diseases, myopathies or tumor metastasis [2,15]. Mutations of β-actin cause pleiotropic diseases and can be linked to neutrophil dysfunction (mutation E364K) [16], malformations, deafness, and delayed-onset dystonia (R183W) [17]. In addition, β-actin

mutations are associated with metastasis [18] and tumours like the diffuse large B-cell lymphoma [19,20]. Multiple missense mutations of γ-actin have been described (T89I, K118M, K118N, I122V, E241K, P264L, T278I, P332A, V370A), all of them are associated with autosomal dominant non-syndromic sensorineural progressive hearing loss [21,22,23,24,25,26,27].

Myosin isoforms are members of a structurally and functionally diverse superfamily of mechanoenzymes. They use actin-activated ATP turnover to trigger cyclic conformational changes leading to force generation and directional movement. Members of the nonmuscle myosin-2 (NM-2) family act as central regulators of the highly dynamic eukaryotic cytoskeleton. In vertebrates, three isoforms can be distinguished: nonmuscle myosin-2a (NM-2A), -2B (NM-2B), and -2C (NM-2C). The complexity of the NM-2 proteome is enhanced by alternative splicing of the NM-2B and -2C isoforms. The enzymatic properties, subcellular and tissue-specific localizations of NM-2 isoforms and their splice variants are distinctive [28,29,30] but they can substitute for each other to a certain extent [31]. NM-2 isoforms are required for cell migration, cell adhesion, vesicle transport, and cytokinesis (reviewed by Heissler and Manstein [32]). NM-2A mutations are associated with congenital macrothrombocytopenia, deafness, progressive nephropathy, and presenile cataracts [33]. In addition, alterations of NM-2A activity or expression level contribute to tumor invasion and [34,35,36] metastasis. NM-2B is only indirectly linked to pathologies including neurodegenerative diseases [32]. Mutations in NM-2C are associated with deafness, distal myopathy and peripheral neuropathy [37,38]. Myosin-7A belongs to the unconventional human myosins. It is involved in mechano-electrical transduction and stereocilia morphogenesis in cochlear hair cells [39,40] and has been associated with lysosomal as well as neuroretinal melanosome, phagosome and opsin trafficking [41,42,43,44]. Mutations of myosin-7A are causative for non-syndromic hearing loss and Usher syndrome type 1B [45,46].

The ability of NM-2 and myosin-7A motors to support multiple functions within the cytosol is closely linked to the occurrence of the cytoplasmic β- and γ-actin. Their common physiological tasks and relation to similar pathologies suggests a special mode of interaction between cytoplasmic actin and myosin isoforms. Here, we describe the modulating effect α-, β- and γ-actin have on the functional properties of cytoplasmic myosins.

Materials and Methods

Reagents

Restriction enzymes, DNA-Polymerase, DNA-modifying enzymes (Fermentas), NHS-Rhodamine labeling reagents (5-(and 6)-carboxytetramethylrhodamine, *N*-Hydroxysuccinimide ester; Pierce Biotechnology), goat anti-mouse horseradish-peroxidase and SuperSignal West Femto Maximum Sensitivity Substrate were purchased from Thermo Fisher Scientific. FRET (Förster resonance energy transfer) labeling dyes and NPE-caged ATP (Adenosine 5′-Triphosphate, P3-(1-(2-Nitrophenyl)Ethyl) Ester) were from Invitrogen (Life Technologies). Penta-His antibody and Ni^{2+}-NTA were purchased from QIAGEN. Standard reagents were from Sigma-Aldrich.

Plasmid construction

The human gelsolin C-terminal half G4-6 was subcloned from shuttle vector pKN172 into the cold-shock expression vector pCOLD II (Takara Bio, Inc.) using the restriction sites for *Bam*HI and *Hind*III after introduction of a polyhistidine tag using the primers 5′-GATCCCATCACCATCATCACCATC ACG -3′ and 5′-GATCCGTGATGGTGATGATGGTGATGG-3′. The

baculovirus transfer vectors for β- and γ-actin were produced as follows. The cDNAs for human cytoplasmic actins were amplified by PCR using the primers: 5′-GCCTCGAGATGGATGATGA-TATCGCCGCG-3′ (N-terminal β-actin), 5′-GCCTCGA-GATGGA AGAAGAGATCGCCGCGCTGGTCATTGA-CAATGGC-3′ (N-terminal γ-actin), and 5′-GCATGCATCTAG AAGCATTTGCGGTGGACG-3′(C-terminal, β- and γ-actin). The DNA fragments were cloned into pFastBac Dual vectors (Invitrogen) by usage of the restriction enzymes *Xho*I and *Nsi*I under the p10 promoter for expression in the baculovirus/*Sf*9 system. The baculovirus transfer vectors encoding the motor domains of human nonmuscle myosin-2A (residues 1–775), -2B (residues 1–782), and -2C1 splice variant (residues 1–807), each fused with two *Dictyostelium discoideum* α-actinin repeats acting as an artificial lever arm and an octahistidin-tag, were generated as described previously [47]. The myosin-7a motor domain construct (amino acids 1–747) was cloned similarly but fused with an EYFP fluorescence marker additionally to the artificial lever arm [48]. The transfer vectors encoding cytoplasmic actins and NM-2 isoforms were transformed in DH10Bac *E. coli* cells to generate recombinant bacmids. After isolation and confirmation by PCR, the respective bacmids were transfected into *Sf*9 (*Spodoptera frugiperda*) insect cells using Cellfectin II (Invitrogen). Recombinant virus was amplified according to the manufacturer's protocol, *Sf*9-cells were infected and harvested 3 days *post infectionem* and stored at −80°C. All plasmids were verified by sequencing. DNA sequences were analyzed in DNASTAR Lasergene Core Suite software (DNAstar, Inc.).

Protein preparation

The C-terminal gelsolin half G4-6 was produced as described by Ohki et al. [49]. Typically, the purification of G4-6 yielded 50–100 mg pure protein per liter *E. coli* culture. Purification of mouse tropomyosin α-1 chain (Tm) was performed according to Coulton et al. [50] and typically yielded 60 mg per liter culture. Tag-free cytoplasmic human β- and γ-actin were purified as G-actin (globular or monomeric actin) by affinity chromatography using the G4-6 gelsolin deletion mutant according to Ohki et al. [49]. Mammalian skeletal muscle α-actin was purified from rabbit as described previously [47,51]. For selected experiments, monomeric α-actin was further purified by G4-6 affinity chromatography as described above. Actins were polymerized by the addition of 2 mM MgCl$_2$ and 0.1 M KCl for 3 h at 21°C and then used in the assay. Actin which was not used immediately was kept on ice until usage for no longer than 3 days. Sufficient polymerization ability of the actin isoforms was checked by sedimentation of F-actin at 100.000 *g* and subsequent SDS-PAGE (sodium dodecyl sulfate polyacrylamide gel electrophoresis) of the supernatant and the pellet, which was resolved in an equal volume. Recombinant human myosin-2A, -2B and 2C1 and myosin-7A constructs were purified as described previously [30,48]. Proteins were supplemented with 3% sucrose (actin, Tm) or 10% trehalose (myosin), flash frozen in liquid N$_2$ and stored at −80°C.

Gel electrophoresis, Immunoblots and IEF

Polyacrylamide gel electrophoresis (10%) in the presence of SDS was used to show the homogeneity of the actin preparations. For immunoblotting, protein samples were separated by SDS-PAGE, transferred onto nitrocellulose membrane and blocked with nonfat dry milk (5% w/v) in TBST (20 mM Tris-HCl pH 7.5, 150 mM NaCl, 0.05% (v/v) Tween-20). The membrane was incubated overnight with monoclonal anti-muscle-actin, anti-β-actin, or anti-γ-actin mouse antibody in TBST (1:1000 dilutions). Monoclonal muscle specific actin antibody Ab-4
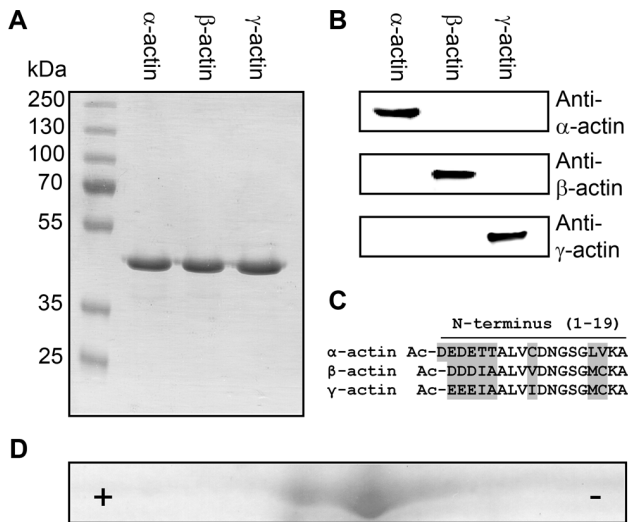
Figure 1. Purification of actin isoforms. (A) SDS-PAGE of purified actin isoforms. (B) Immunoblot-based identification of actin isoforms. The actin antibodies used show no cross-reactivity. (C) Actin isoforms display subtle differences primarily located at their N-terminus as shown in the protein sequence alignment. Sequence variations at the N-terminus of α-, β- and γ-actin are marked in grey. Mature actin isoforms are acetylated (Ac) at their N-terminus (D) 2D-gelelectrophoresis of purified γ-actin (IEP 5.31) containing ~10% co-purified insect actin (IEP 5.29). The acidic (+) and the basic end (−) are marked.
doi:10.1371/journal.pone.0070636.g001

(mouse, clone HHF35) was from Thermo Fisher Scientific, monoclonal anti-β-actin (mouse, clone AC-74) and anti-γ-actin (mouse, clone 2-2.1.14.17) antibody were purchased from Sigma-Aldrich. After washing with TBST it was kept for 1 h at room temperature with horseradish peroxidase conjugated secondary

antibody. Detection was performed by means of chemiluminescence. Isoelectric focusing (IEF) electrophoresis (pH range 4–7) was performed using the ZOOM IPGRunner Kit (Life Technologies) according to the manufacturer's protocol.

LC-MS analysis

Sample preparation and processing (liquid chromatography, LC) for mass spectrometry (MS) analysis was performed as described previously [52] with the exception that proteins were alkylated by addition of 2% acrylamide. Peptide samples were separated with a nano-flow ultra-high pressure liquid chromatography system (RSLC, Thermo Scientific). The RSLC system was coupled online via a Nano Spray Flex Ion Source II to an LTQ-Orbitrap Velos mass spectrometer (both from Thermo Scientific). Raw data were processed using Proteome Discoverer software (version 1.2, Thermo Scientific), the Mascot search engine and human entries of the SwissProt/Uniprot database. Acetylation, oxidation, deamidation, arginylation and propionylation were used as possible modifications. Peptides with a peptide ion score above 30 and a false discovery rate below 0.05 were considered.

FRET experiments

Fluorescence labeling of α-, β-, and γ-actin and FRET copolymerization assay were performed as follows. Each isoform was independently labeled with 1,5-IAEDANS (5-((((2-Iodoacetyl)amino)ethyl)amino) Naphthalene-1-Sulfonic Acid, $\lambda_{\text{Emission,max}} = 490$ nm) and 5-IAF (5-Iodoacetamidofluorescein, $\lambda_{\text{Emission,max}} = 520$ nm). Briefly, 1 mg/ml monomeric actin in G-actin buffer (10 mM Tris-HCl pH 8.0, 0.2 mM CaCl$_2$, 1 mM DTT, 0.5 mM ATP) was mixed with 5-fold molar excess of labeling dye and incubated at room temperature for 4 hours. After polymerization (see also *protein preparation*), F-actin was pelleted by centrifugation at 100.000 g for 3 hours. The resulting pellets were homogenized in G-actin buffer and incubated at 4°C over night. To remove actin
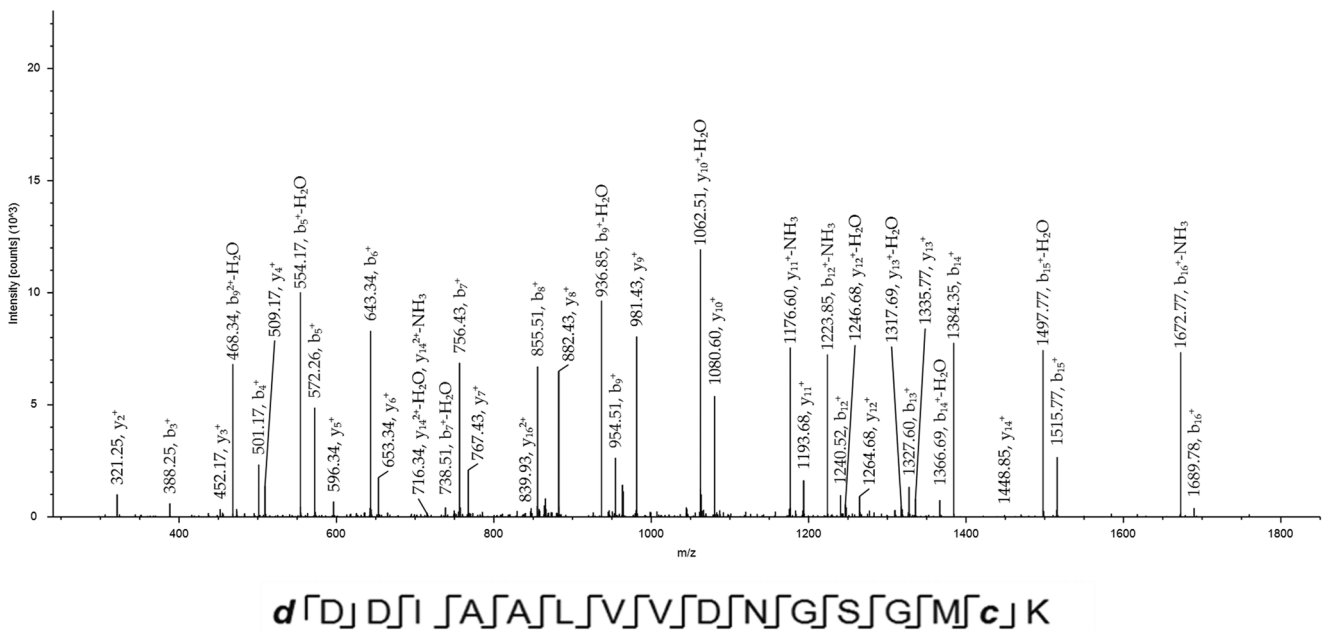
Figure 2. β- and γ-actin are N-terminally acetylated. Mass spectrum of the N-terminal peptide of β-actin. The protonated molecular ion (MH$^+$) of the identified peptide has a mass of 1835.8 Da and is modified by removal of Met1 (m = 1722.9 Da), acetylation of Asp1 (indicated as d, Δm = +42 Da) and due to sample processing by an artificial propionamidation of cysteine (indicated as c, Δm = +71 Da). Similar results were obtained with γ-actin (spectrum not shown).
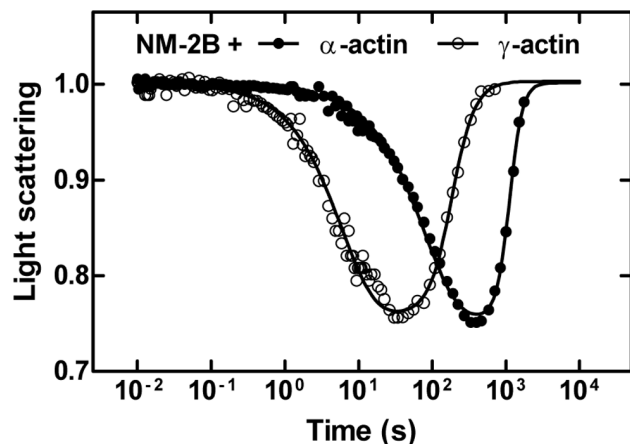doi:10.1371/journal.pone.0070636.g002

unable to depolymerize the solution was centrifuged at 100.000 g for 1 hour. The G-actin concentration in the supernatant and the extent of actin labeling were determined according to the manufacturer's protocol. Finally, an equimolar mixture of 1,5-IAEDANS and 5-IAF labeled actin was polymerized and fluorescence emission spectra were measured at a concentration of 1.3 µM in an Varian Cary Eclipse spectrofluorometer ($\lambda_{\text{Excitation,IAEDANS}}$ = 336 nm).

ATPase measurements

Comparative steady-state kinetics of the various myosin isoforms stimulated by α-, β-, and γ-actin homopolymers or copolymers were measured with the NADH-coupled assay as described previously [53]. Using an ATP regeneration system consisting of 0.05 mg/ml pyruvate kinase, 0.5 mM phosphoenolpyruvate, 0.02 mg/ml lactate dehydrogenase measurements were performed at 25°C in a buffer containing 25 mM HEPES (pH 7.4), 5 mM MgCl$_2$, 0.2 mM NADH, 1 mM ATP and 0.5 mM DTT. Myosin concentrations were varied between 0.2 and 1.0 µM and F-actin from 0–100 µM. Following the NADH oxidation by measuring the decrease in absorption at 340 nm ($\varepsilon = 6220$ M^{-1} cm^{-1}), the ATPase rates were determined by linear curve fitting and the basal ATPase activity of myosin was subtracted from the actin-activated data.

Flash photolysis experiments

Transient kinetic measurements were performed at 30°C using a flash photolysis system as described previously [54]. 1 µM myosin was mixed with 5 µM F-actin and 0.5 mM caged-ATP (cATP) in a buffer containing 50 mM KP$_i$ pH 7.4, 400 mM KCl, 5 mM MgCl$_2$ and 10 mM DTT. The third harmonics (355 nm) of a Surelite II-10 NdYAG laser was used for photolysis of cATP. The amount and time of ATP release was monitored from the increase of absorbance at 405 nm due to the formation of the

excited aci-nitro intermediate. The minimal concentration of free ATP was at least 5-fold higher than the myosin concentration. This allows analysis of the reaction within pseudo-first order approximation. ATP induced dissociation of myosin from F-actin and following reassociation after full hydrolysis of ATP was monitored as the change of light scattering signal ($\lambda > 400$ nm).

In vitro motility assay

F-Actin isoforms were stabilized and visualized by decoration with fluorescently labeled Tm-dimers because the behavior of native actin filaments in their interaction with NM-2 isoforms can
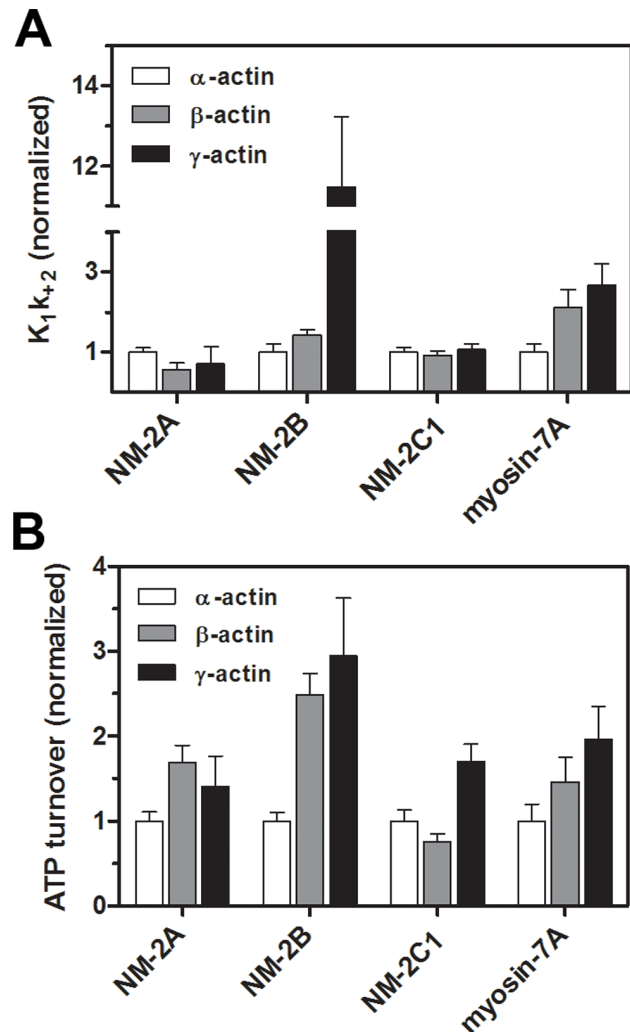
Figure 4. Flash photolysis experiments with nonmuscle myosin and actin isoforms. (A) The graphs show the relative changes of the apparent second order rate constants K_1k_{+2}. P-values of unpaired t-tests were <0.05 for the combinations NM-2A (α- and β-actin), NM-2B (α- and β-/γ-actin), and myosin-7A (α- and β-/γ-actin). (B) ATP turnover rates of nonmuscle myosin isoforms interacting with β- or γ-actin. P-values of unpaired t-tests were <0.05 for the combinations NM-2A (α- and β-/γ-actin), NM-2B (α- and β-/γ-actin), NM-2C1 (γ- and α-/β-actin), and myosin-7A (all combinations). Rates were normalized using α-actin as a reference. The ATP-induced dissociation is accelerated for the complexes NM-2B/β-/γ-actin and myosin-7A/β-/γ-actin. The interaction of cytoplasmic actins and NM-2 or myosin-7A isoforms leads to 2- to 3-fold increased catalytic activities. Reference values for K_1k_{+2} (µM^{-1} s^{-1}) as determined with α-actin are as follows: NM-2A, 0.14±0.003; NM-2B, 0.24±0.02; NM-2C1, 0.89±0.01; myosin-7A, 0.44±0.01 (see also [32,48]). doi:10.1371/journal.pone.0070636.g004

Figure 3. Time-dependent dissociation and association of NM-2B from filamentous α- and γ-actin. The light scattering signal normalized to the initial value shows the time-dependent dissociation and association of the actomyosin complex formed by NM-2B and α- or γ-actin. The initial drop in the light scattering signal follows the release of ATP from caged-ATP by a flash of UV-laser. The single exponential reduction in scattering intensity monitors the ATP-induced dissociation of myosin from F-actin. The following restoration of the light scattering signal is caused by rebinding of myosin to the actin filament after ATP hydrolysis is completed. As shown for NM-2B, γ-actin causes faster dissociation and association compared to α-actin. Note the logarithmic time scale on the graph. doi:10.1371/journal.pone.0070636.g003

be altered when stabilized with phalloidin [47]. The labeling was performed using the NHS-Rhodamine Labeling Kit (Pierce) according to the manufacturer's protocol. Using assay buffer AB (25 mM Imidazole pH 7.4, 25 mM KCl, 4 mM MgCl$_2$, 1 mM EGTA), 10 μM F-actin (α-, β-, and γ-actin, respectively) was incubated with an equimolar amount of labeled Tm for at least 1 h at 21°C or overnight on ice. The actin-Tm complex was then sedimented at 100.000 g for 30 min, washed with AB-buffer and gently resuspended with the same buffer by thorough pipetting. The complex was diluted to 50 nM F-actin directly before usage. Standard in vitro motility assays were performed at 30°C using an Olympus IX70 inverted fluorescence microscope according to published protocols [30,55]. Myosin concentration in the assay was 1 mg/ml. Inactive myosin heads were removed by actin affinity purification. We increased the incubation time of Tm-actin with myosin to 10 min and included 0.5% methylcellulose to prevent diffusion of Tm away from actin and Tm-actin from the myosin substratum [56]. The movement of at least 150 actin filaments per observation area was recorded over a length of 50 frames with an exposure time of 1000 ms and a cycle time of 2000 ms using CellR Software version 2.8 (Olympus). Automated actin filament tracking was performed with the program DiaTrack 3.02 (Semasopht/INDEC Biosystems) and the average sliding velocity was determined by analysis of the Gaussian distribution with Origin 8.5 (OriginLab).

Computational and statistical analysis

Data analysis and graph plotting were performed using Origin 8.5 (OriginLab) and GraphPad Prism version 5.02 (GraphPad Software). Unpaired t-test was employed for statistical analysis of the in vitro motility data using GraphPad Prism. If not otherwise specified, each single measure was repeated at least three times and errors were calculated as standard errors.

Results

The cytoplasmic actin isoforms were produced in Sf9 cells and purified to homogeneity (Figure 1A). Immunoblots were used to verify the purity of the particular isoactins (Figure 1B). Although actin isoforms display only subtle N-terminal differences (Figure 1C), the monoclonal antibodies used are highly specific for this region and show no cross-reactivity with other isoactins. IEF was performed to determine the amount of contaminating insect actin. Due to differences in their isoelectric points (IEP), the more basic γ-actin (IEP 5.31) can be separated from the more acidic insect actin (IEP 5.29) as depicted in Figure 1D. Insect and human β-actin have similar IEPs and separate less well. IEF and MS analyses indicate that the level of contamination of human cytoplasmic actins with endogenous actin from insect cells is in the range of 5–15% (N = 3).

The purified recombinant proteins are identical in sequence to the native actin isoforms. MS analyses showed that both recombinant actin isoforms purified from Sf9 cells are post-
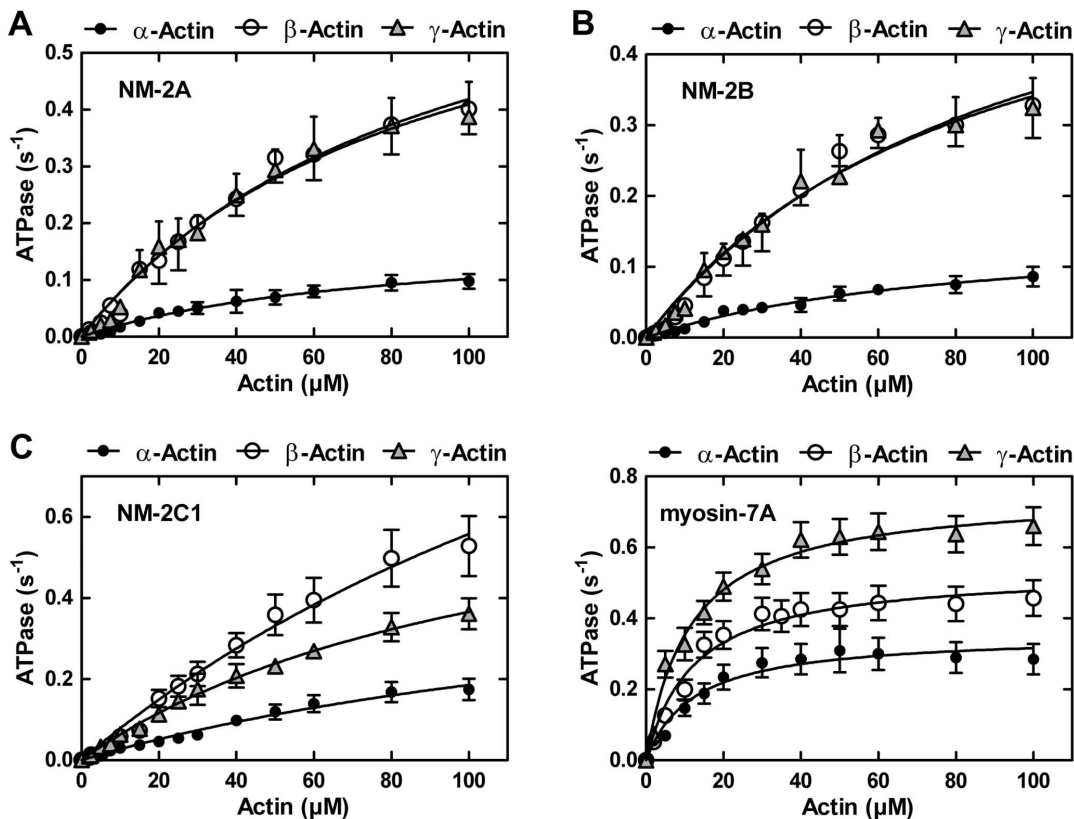
Figure 5. Cytoplasmic actins enhance nonmuscle myosin-2 and myosin-7A efficiency. Steady-state ATPase activities of (A) NM-2A, (B) NM-2B, (C) NM-2C1 and (D) myosin-7A measured as a function of actin concentration (α-, β-, and γ-F-actin). The ATPase activity in the absence of F-actin was subtracted from the actin-activated data. Values for K_{actin} and k_{cat} were calculated from a hyperbolic fit (ATPase activity = (k_{cat} [F-actin])/(K_{actin}+[F-actin])) to the data (see Table 1).
doi:10.1371/journal.pone.0070636.g005

translationally modified at their N-terminus. We identified trypsin digested β-actin with a sequence coverage of >99% (56 peptides, score 56,000) and γ-actin with a coverage of >93% (52 peptides, score 59,000). The predominant species (>95%) has undergone N-terminal removal of Met[1] and acetylation at Asp[2] (β-actin) or Glu[2] (γ-actin). Additionally, we detected N-terminal peptides with residual amounts (<5%) of acetylated Met[1], a modification required for removal of the first residue. A mass spectrum of the modified N-terminal peptide from β-actin is shown in Figure 2.

ATP induced dissociation and turnover kinetics of specific actomyosin complexes

We used flash photolysis of an inert ATP precursor (caged-ATP) to initiate the dissociation of NM-2/F-actin and myosin-7A/F-actin complexes and subsequent reaction stages (Figure 3). The fast dissociation of the actomyosin complex upon ATP binding can be monitored by light scattering, which is highly sensitive to changes in size and molar mass of protein complexes. The apparent dissociation rate constant k_{obs} was obtained by fitting the data to a single exponential function. The ATP concentration released by each flash and the associated values for k_{obs} were determined and used to calculate the apparent second order rate constant K_1k_{+2} for nucleotide induced dissociation of the actomyosin complex. K_1 is the fast diffusion limited equilibrium constant for ternary complex formation. ATP binding is followed by an irreversible conformational transition of myosin (k_{+2}). Once the hydrolysis of the released ATP has been completed, the actomyosin complex reforms at the end of an extended steady-state phase. The transition from steady-state was approximated by a sigmoidal curve and the midpoint was used for calculation of the ATP turnover rate. The resulting values for K_1k_{+2} and ATP

turnover, as measured with 5 µM F-actin, are summarized in Figure 4A and 4B. Compared to the situation observed in the presence of α-actin, NM-2B and myosin-7A show 11-fold and ~2-fold increases in K_1k_{+2} in the presence γ-actin. In the case of myosin-7A, a ~2-fold increase was also observed in the presence of β-actin. The rate of ATP-induced dissociation of complexes comprising NM-2A and -2C1 is not increased if α-actin is replaced by β- or γ-actin. With regard to ATP hydrolysis rates, almost all myosin isoforms tested display a significant increase in the presence of the cytoplasmic isoactins. The largest change was observed for the combination NM-2B/γ-actin, showing a 3-fold increase in ATP turnover (Figure 4B). Only the combination of NM-2C1 with β-actin showed no increase in ATP turnover.

Cytoplasmic actins enhance the coupling efficiencies of NM-2 and myosin-7A

Steady-state ATPase measurements of NM-2 and myosin-7A in the presence of 1–100 µM filamentous α-, β- and γ-actin were performed to determine the maximal ATP turnover rate (k_{cat}), the actin concentration required for half-maximal activation (K_{actin}), and the apparent second order rate constant for F-actin binding in the presence of ATP (k_{cat}/K_{actin}). Based on the values determined for k_{cat}, β-actin is 3 to 4-fold more potent in the activation of ATP turnover by NM-2 isoforms than α-actin (Figure 5, Table 1). The level of activation induced by γ-actin is 1.5-fold (NM-2C1) and 4-fold (NM-2A and -2B) greater compared to α-actin. The choice of isoactins interacting with NM-2 isoforms appears to have only a minor effect on K_{actin}. However, due to the high K_{actin}-values displayed by the NM-2 isoforms and technical limitations of the assay, the respective values should be treated only as rough estimates [30]. For each actomyosin combination, we determined the second order rate constant k_{cat}/K_{actin} (µM^{-1} s^{-1}), which is a direct measure of the coupling efficiency between the actin– and nucleotide–binding sites of myosin. Values for k_{cat}/K_{actin} can be determined accurately at actin concentrations much smaller than K_{actin} from the initial slope of the Michaelis-Menten-plot (Figure 5 and Table 1). The coupling efficiencies of NM-2 isoforms with β- or γ-actin are significantly greater (2-fold to 4-fold) compared to α-actin. The stimulation of myosin-7A ATPase and its coupling efficiency (Figure 5, Table 1) is highest with γ-actin (2-to 3-fold over α-actin).

NM-2 isoforms slide cytoplasmic β- and γ-actin at higher velocities than α-skeletal actin

Fluorescently labeled Tm was used to visualize and stabilize F-actin. The results of in vitro motility experiments that were performed with Tm decorated F-actin show that β- and γ-actin support significantly higher motile activity (10–25%) of NM-2A, -2B and -2C1, compared to the velocities observed in the presence of α-actin (Table 2). The sliding velocity of each actomyosin

Table 1. Summary of steady-state kinetic parameters of NM-2A, -2B, -2C1 and myosin-7A activated by actin isoforms.

		α-actin	β-actin	γ-actin
NM-2A	$K_{app,actin}$ (µM)	80.2±11.5	94.6±16.6	88.0±16.2
	k_{cat} (s^{-1})	0.18±0.01	0.81±0.08	0.77±0.08
	Coupling efficiency*	0.002±0.0005	0.008±0.001	0.008±0.001
NM-2B	$K_{app,actin}$ (µM)	82.0±13.9	95.1±20.2	86.9±16.8
	k_{cat} (s^{-1})	0.15±0.01	0.67±0.08	0.63±0.07
	Coupling efficiency*	0.002±0.001	0.007±0.001	0.007±0.001
NM-2C1	$K_{app,actin}$ (µM)	>100	>100	>100
	k_{cat}** (s^{-1})	0.17±0.02	0.53±0.07	0.36±0.04
	Coupling efficiency*	0.003±0.0005	0.007±0.001	0.006±0.001
Myosin-7A	$K_{app,actin}$ (µM)	12.3±2.3	12.3±1.8	11.3±1.2
	k_{cat} (s^{-1})	0.35±0.01	0.53±0.02	0.75±0.02
	Coupling efficiency*	0.02±0.001	0.04±0.0015	0.06±0.001

*The second order rate constant $k_{cat}/K_{app,actin}$ (µM^{-1} s^{-1}) indicates the coupling efficiency and was obtained from the initial slope of the steady-state ATPase activity versus actin concentration plot.
**Activities of NM-2C1 isoforms in the presence of 100 µM F-actin. With regard to k_{cat}, p-values of unpaired t-tests were ≤0.01 for the combinations α- and β-/γ-actin for all NM-2 isoforms and myosin-7A.
The k_{cat}-values for β- and γ-actin were different for NM-2C1 (p = 0.025) and myosin-7A (p = 0.005). No significant differences were found for $K_{app,actin}$ (p≥0.25 for all combinations). Coupling efficiencies differ significantly (p≤0.05) between α-actin and cytoplasmic actins for all myosin isoforms shown in the table. The coupling efficiencies of β- and γ-actin were different for myosin-7A (p<0.001).
doi:10.1371/journal.pone.0070636.t001

Table 2. Motility rates of NM-2 and actin isoforms.

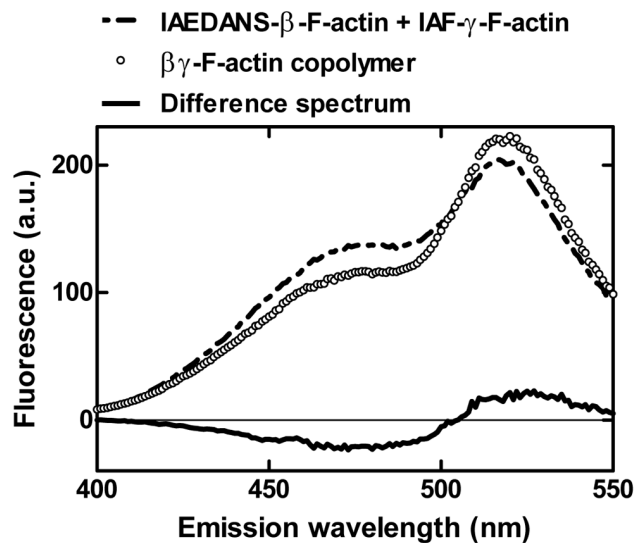| Motility rates (nm s^{-1})	α-actin	β-actin	γ-actin
NM-2A	76.3±3.0 (N = 11)	84.2±1.2 (N = 11)	94.6±2.9 (N = 8)
NM-2B	30.1±0.5 (N = 9)	35.2±0.8 (N = 10)	32.7±1.0 (N = 8)
NM-2C1	51.7±2.1 (N = 13)	60.9±1.1 (N = 21)	61.2±1.1 (N = 13)

Motility rates of myosin-7A with actin isoforms were not determined. N: number of experiments, errors indicate S.E.M.
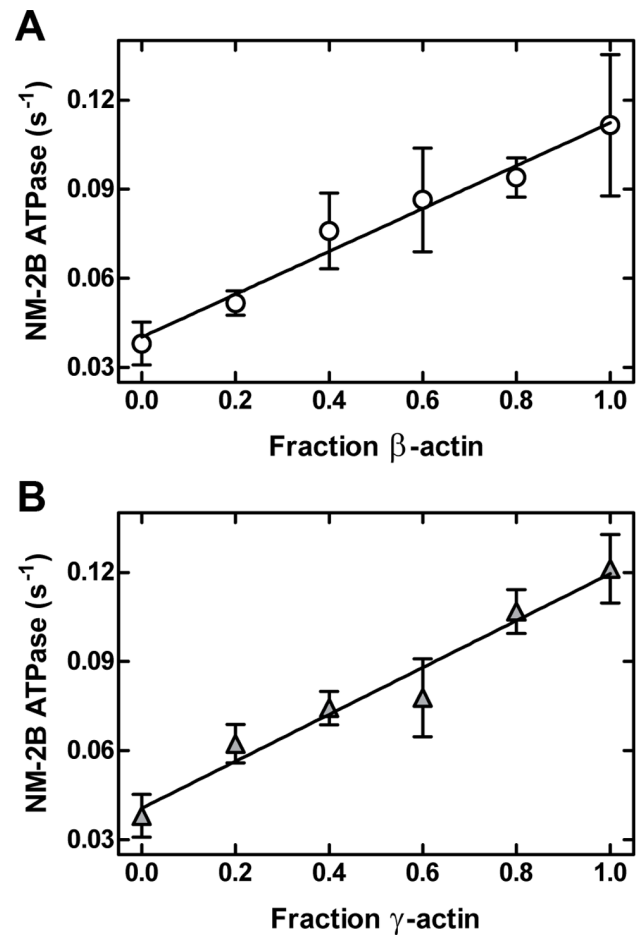doi:10.1371/journal.pone.0070636.t002

combination was repeatedly determined in fresh flow cells and the mean ± S.E.M. was calculated. P-values of unpaired *t*-tests were <0.05 for the combinations NM-2A/β-actin and NM-2A/γ-actin and <0.01 for all other combination of NM-2 with β- or γ-actin when compared to the respective NM-2/α-actin complexes.

Formation and functional behavior of isoactin copolymers

To investigate the ability of isoactins to copolymerize, we performed fluorescence resonance energy transfer (FRET) assays using pairs of IAEDANS and IAF labeled isoactins. The isoactins copolymerized readily *in vitro*. Figure 6 shows the fluorescence spectrum of a mixture of the separately polymerized labeled actin isoforms, the spectrum obtained after copolymerization of IAEDANS-β-actin and IAF-γ-actin, and the associated difference spectrum. After copolymerization a marked reduction of the donor fluorescence and an increase of IAF fluorescence were observed. The filaments that result from mixing equimolar concentrations of labeled isoactins, display transfer efficiencies of 10–30% (Table 3). To analyze whether these hybrid filaments display an intermediate behavior or are dominated by the functional behavior of one isoactin, we examined how changes in isoform composition affect the activation of NM-2B ATPase activity. We copolymerized α-actin with β- and γ-actin respectively at increasing ratios (0, 0.2, 0.4, 0.6, 0.8, and 1.0) and used 20 μM copolymer solutions to stimulate NM-2B ATPase activity. Because the FRET copolymerization analysis did not show a preference for one particular isoactin to form homopolymers, we assume that the resulting filaments consist of randomly distributed α- and β-/γ-monomers. The catalytic activity which these mixed filaments support increases linearly with increasing β- or γ-actin content (Figure 7A and 7B).

Figure 7. Activation of NM-2B ATPase rate by αβ- and αγ-actin copolymers. Copolymers with different mixing ratios were used to stimulate the ATPase activity of NM-2B. Measurements were performed using a final concentration of 20 μM F-actin.
doi:10.1371/journal.pone.0070636.g007

Discussion

Our results show clear increases in actin-activation and functional competence for all nonsarcomeric myosins tested, when they were allowed to interact with cytoplasmic isoactins instead of α-actin. The preferred interaction of NM-2A, -2B and -2C1 with cytoplasmic β-actin and γ-actin fits well to the proteins' overlapping functions in cell migration, adhesion, cytokinesis, and cytoskeletal maintenance [3,32,57]. In regard to their interaction with β- or γ-actin, only NM-2A and NM-2B show no clear preference for either cytoplasmic isoactin. In our *in vitro*

Figure 6. FRET copolymerization analysis of actin isoforms. Fluorescence emission spectra of IAEDANS-β-actin and IAF-γ-actin, both separately polymerized and after copolymerization. The donor fluorescence (IAEDANS) peaks around 490 nm and decreases significantly upon copolymerization whereas the fluorescence of the acceptor (IAF) at 520 nm apparently increases as shown in the difference spectrum.
doi:10.1371/journal.pone.0070636.g006

Table 3. FRET efficiencies of copolymerized actin isoforms.

E (%)	IAEDANS-α-actin	IAEDANS-β-actin	IAEDANS-γ-actin
IAF-α-actin	29.5	33.7	23.1
IAF-β-actin	8.7	16.0	9.8
IAF-γ-actin	13.0	25.2	15.0

Transfer efficiencies (E) were measured as the relative donor fluorescence intensity in the presence (F_{DA}) and absence (F_D) of the acceptor $E = (1 - F_{DA}/F_D)/LD_A$ where LD_A is the labeling degree of the acceptor.
doi:10.1371/journal.pone.0070636.t003

experiments, myosin-7A showed a distinct preference for γ-actin over β-actin. In their proper physiological context, myosin-7A, β- and γ-actin play a key role in the development, function and maintenance of cochlear hair cell stereocilia [14,39]. Although the presence of both cytoplasmic actin isoforms is required for regular hair cell development, differences in the pattern of progressive hearing loss are observed upon their selective ablation. It was reported that γ-actin may be more abundant in particular hair cell structures and that the severity of progressive hearing loss can be related to the γ-actin concentration [14]. Further evidence for specific intracellular interactions between myosin-7A and γ-actin has been provided by studies of *MYO7A* gene defects [45,46] and γ-actin mutations [21,22,23,24,25,26,27]. Our results pointing at a preferred interaction of the proteins provide an explanation why both sets of gene defects lead to similar phenotypes. NM-2C also plays a role in the function and maintenance of stereocilia. Mutations in NM-2C are associated with hereditary deafness (DFNA4) [37]. Genome-wide linkage analysis identified an autosomal-dominant mutation which causes a complex phenotype associated with peripheral neuropathy, myopathy, hoarseness, and hearing loss [58]. The results of our *in vitro* assays show that different from myosin-7A, NM-2C shows a clear preference for β-actin over γ-actin.

Although copolymerization of isoactins has only been studied for selected cell types, it is generally assumed that copolymers do not commonly exist *in vivo*. The basis for their discrete polymerization and localization remains to be determined, as FRET-based analysis confirms that *in vitro* isoactins do efficiently copolymerize [59]. Moreover, measurements with αβ-actin and αγ-actin copolymers indicate linear relationship between mixing ratio and isoform composition and the observed ATPase activity

and the isoform composition of the copolymers. The behaviour of a hybrid F-actin can be reduced to the proportional representation of the isoforms suggesting that each actin acts independently from its neighbours.

Our results show that isoactins modulate the function of nonsarcomeric myosins in discrete ways. The observed differences in the interaction of individual actin and myosin isoforms are likely to be further enhanced by the impact of differential posttranslational modifications and interactions with regulatory actin binding proteins such as tropomyosin. Arginylation, which occurs in ~40% of β-actin but not γ-actin, affects β-actin polymerization, localization, and lamella formation [60]. Furthermore, tropomyosin isoforms such as Tm5NM1 and TmBr3 show preferred interaction patterns with cytoplasmic isoactins and alter the recruitment and activity of NM-2 motors [61,62].

Author Contributions

Conceived and designed the experiments: MM RPD MT DJM. Performed the experiments: MM RPD IC. Analyzed the data: MM RPD IC DJM. Contributed reagents/materials/analysis tools: MM RPD PC MT SMH. Wrote the paper: MM DJM. Critical Discussion: MP.

References

1. Vandekerckhove J, Weber K (1978) At least six different actins are expressed in a higher mammal: an analysis based on the amino acid sequence of the amino-terminal tryptic peptide. J Mol Biol 126: 783–802.
2. Tondeleir D, Vandamme D, Vandekerckhove J, Ampe C, Lambrechts A (2009) Actin isoform expression patterns during mammalian development and in pathology: insights from mouse models. Cell Motil Cytoskeleton 66: 798–815.
3. Dugina V, Zwaenepoel I, Gabbiani G, Clement S, Chaponnier C (2009) Beta and gamma-cytoplasmic actins display distinct distribution and functional diversity. J Cell Sci 122: 2980–2988.
4. Hoock TC, Newcomb PM, Herman IM (1991) Beta actin and its mRNA are localized at the plasma membrane and the regions of moving cytoplasm during the cellular response to injury. J Cell Biol 112: 653–664.
5. von Arx P, Bantle S, Soldati T, Perriard JC (1995) Dominant negative effect of cytoplasmic actin isoproteins on cardiomyocyte cytoarchitecture and function. J Cell Biol 131: 1759–1773.
6. Pollard TD, Borisy GG (2003) Cellular motility driven by assembly and disassembly of actin filaments. Cell 112: 453–465.
7. Chesarone MA, Goode BL (2009) Actin nucleation and elongation factors: mechanisms and interplay. Curr Opin Cell Biol 21: 28–37.
8. Kaech S, Fischer M, Doll T, Matus A (1997) Isoform specificity in the relationship of actin to dendritic spines. J Neurosci 17: 9565–9572.
9. Mounier N, Perriard JC, Gabbiani G, Chaponnier C (1997) Transfected muscle and non-muscle actins are differentially sorted by cultured smooth muscle and non-muscle cells. J Cell Sci 110 (Pt 7): 839–846.
10. Kumar A, Crawford K, Close L, Madison M, Lorenz J, et al. (1997) Rescue of cardiac alpha-actin-deficient mice by enteric smooth muscle gamma-actin. Proc Natl Acad Sci U S A 94: 4406–4411.
11. Fyrberg EA, Fyrberg CC, Biggs JR, Saville D, Beall CJ, et al. (1998) Functional nonequivalence of Drosophila actin isoforms. Biochem Genet 36: 271–287.
12. Schevzov G, Lloyd C, Gunning P (1992) High level expression of transfected beta- and gamma-actin genes differentially impacts on myoblast cytoarchitecture. J Cell Biol 117: 775–785.
13. Khaitlina SY (2001) Functional specificity of actin isoforms. Int Rev Cytol 202: 35–98.
14. Perrin BJ, Sonnemann KJ, Ervasti JM (2010) beta-actin and gamma-actin are each dispensable for auditory hair cell development but required for Stereocilia maintenance. PLoS Genet 6: e1001158.
15. Chaponnier C, Gabbiani G (2004) Pathological situations characterized by altered actin isoform expression. J Pathol 204: 386–395.
16. Nunoi H, Yamazaki T, Tsuchiya H, Kato S, Malech HL, et al. (1999) A heterozygous mutation of beta-actin associated with neutrophil dysfunction and recurrent infection. Proc Natl Acad Sci U S A 96: 8693–8698.
17. Procaccio V, Salazar G, Ono S, Styers ML, Gearing M, et al. (2006) A mutation of beta-actin that alters depolymerization dynamics is associated with autosomal dominant developmental malformations, deafness, and dystonia. Am J Hum Genet 78: 947–960.
18. Taniguchi S, Kawano T, Kakunaga T, Baba T (1986) Differences in expression of a variant actin between low and high metastatic B16 melanoma. J Biol Chem 261: 6100–6106.
19. Leavitt J, Ng SY, Varma M, Latter G, Burbeck S, et al. (1987) Expression of transfected mutant beta-actin genes: transitions toward the stable tumorigenic state. Mol Cell Biol 7: 2467–2476.
20. Lohr JG, Stojanov P, Lawrence MS, Auclair D, Chapuy B, et al. (2012) Discovery and prioritization of somatic mutations in diffuse large B-cell lymphoma (DLBCL) by whole-exome sequencing. Proc Natl Acad Sci U S A 109: 3879–3884.
21. van Wijk E, Krieger E, Kemperman MH, De Leenheer EM, Huygen PL, et al. (2003) A mutation in the gamma actin 1 (ACTG1) gene causes autosomal dominant hearing loss (DFNA20/26). J Med Genet 40: 879–884.
22. Zhu M, Yang T, Wei S, DeWan AT, Morell RJ, et al. (2003) Mutations in the gamma-actin gene (ACTG1) are associated with dominant progressive deafness (DFNA20/26). Am J Hum Genet 73: 1082–1091.
23. Rendtorff ND, Zhu M, Fagerheim T, Antal TL, Jones M, et al. (2006) A novel missense mutation in ACTG1 causes dominant deafness in a Norwegian DFNA20/26 family, but ACTG1 mutations are not frequent among families with hereditary hearing impairment. Eur J Hum Genet 14: 1097–1105.
24. Bryan KE, Wen KK, Zhu M, Rendtorff ND, Feldkamp M, et al. (2006) Effects of human deafness gamma-actin mutations (DFNA20/26) on actin function. J Biol Chem 281: 20129–20139.
25. Liu P, Li H, Ren X, Mao H, Zhu Q, et al. (2008) Novel ACTG1 mutation causing autosomal dominant non-syndromic hearing impairment in a Chinese family. J Genet Genomics 35: 553–558.
26. Morin M, Bryan KE, Mayo-Merino F, Goodyear R, Mencia A, et al. (2009) In vivo and in vitro effects of two novel gamma-actin (ACTG1) mutations that cause DFNA20/26 hearing impairment. Hum Mol Genet 18: 3075–3089.
27. Kruth KA, Rubenstein PA (2012) Two Deafness-causing (DFNA20/26) Actin Mutations Affect Arp2/3-dependent Actin Regulation. J Biol Chem 287: 27217–27226.

28. Wang F, Kovacs M, Hu A, Limouze J, Harvey EV, et al. (2003) Kinetic mechanism of non-muscle myosin IIB: functional adaptations for tension generation and maintenance. J Biol Chem 278: 27439–27448.

29. Kovacs M, Wang F, Hu A, Zhang Y, Sellers JR (2003) Functional divergence of human cytoplasmic myosin II: kinetic characterization of the non-muscle IIA isoform. J Biol Chem 278: 38132–38140.

30. Heissler SM, Manstein DJ (2011) Comparative kinetic and functional characterization of the motor domains of human nonmuscle myosin-2C isoforms. J Biol Chem 286: 21191–21202.

31. Wang A, Ma X, Conti MA, Adelstein RS (2011) Distinct and redundant roles of the non-muscle myosin II isoforms and functional domains. Biochem Soc Trans 39: 1131–1135.

32. Heissler SM, Manstein DJ (2012) Nonmuscle myosin-2: mix and match. Cell Mol Life Sci.

33. Pecci A, Panza E, Pujol-Moix N, Klersy C, Di Bari F, et al. (2008) Position of nonmuscle myosin heavy chain IIA (NMMHC-IIA) mutations predicts the natural history of MYH9-related disease. Hum Mutat 29: 409–417.

34. Derycke L, Stove C, Vercoutter-Edouart AS, De Wever O, Dolle L, et al. (2011) The role of non-muscle myosin IIA in aggregation and invasion of human MCF-7 breast cancer cells. Int J Dev Biol 55: 835–840.

35. Xia ZK, Yuan YC, Yin N, Yin BL, Tan ZP, et al. (2012) Nonmuscle myosin IIA is associated with poor prognosis of esophageal squamous cancer. Dis Esophagus 25: 427–436.

36. Ivkovic S, Beadle C, Noticewala S, Massey SC, Swanson KR, et al. (2012) Direct inhibition of myosin II effectively blocks glioma invasion in the presence of multiple mitogens. Mol Biol Cell 23: 533–542.

37. Donaudy F, Snoeckx R, Pfister M, Zenner HP, Blin N, et al. (2004) Nonmuscle myosin heavy-chain gene MYH14 is expressed in cochlea and mutated in patients affected by autosomal dominant hearing impairment (DFNA4). Am J Hum Genet 74: 770–776.

38. Choi BO, Kang SH, Hyun YS, Kanwal S, Park SW, et al. (2011) A complex phenotype of peripheral neuropathy, myopathy, hoarseness, and hearing loss is linked to an autosomal dominant mutation in MYH14. Hum Mutat 32: 669–677.

39. Self T, Mahony M, Fleming J, Walsh J, Brown SD, et al. (1998) Shaker-1 mutations reveal roles for myosin VIIA in both development and function of cochlear hair cells. Development 125: 557–566.

40. Kros CJ, Marcotti W, van Netten SM, Self TJ, Libby RT, et al. (2002) Reduced climbing and increased slipping adaptation in cochlear hair cells of mice with Myo7a mutations. Nat Neurosci 5: 41–47.

41. Soni LE, Warren CM, Bucci C, Orten DJ, Hasson T (2005) The unconventional myosin-VIIa associates with lysosomes. Cell Motil Cytoskeleton 62: 13–26.

42. Liu X, Ondek B, Williams DS (1998) Mutant myosin VIIa causes defective melanosome distribution in the RPE of shaker-1 mice. Nat Genet 19: 117–118.

43. Gibbs D, Kitamoto J, Williams DS (2003) Abnormal phagocytosis by retinal pigmented epithelium that lacks myosin VIIa, the Usher syndrome 1B protein. Proc Natl Acad Sci U S A 100: 6481–6486.

44. Liu X, Udovichenko IP, Brown SD, Steel KP, Williams DS (1999) Myosin VIIa participates in opsin transport through the photoreceptor cilium. J Neurosci 19: 6267–6274.

45. Weil D, Blanchard S, Kaplan J, Guilford P, Gibson F, et al. (1995) Defective myosin VIIA gene responsible for Usher syndrome type 1B. Nature 374: 60–61.

46. Hildebrand MS, Thorne NP, Bromhead CJ, Kahrizi K, Webster JA, et al. (2010) Variable hearing impairment in a DFNB2 family with a novel MYO7A missense mutation. Clin Genet 77: 563–571.

47. Diensthuber RP, Muller M, Heissler SM, Taft MH, Chizhov I, et al. (2011) Phalloidin perturbs the interaction of human non-muscle myosin isoforms 2A and 2C1 with F-actin. FEBS Lett 585: 767–771.

48. Heissler SM, Manstein DJ (2012) Functional characterization of the human myosin-7a motor domain. Cell Mol Life Sci 69: 299–311.

49. Ohki T, Ohno C, Oyama K, Mikhailenko SV, Ishiwata S (2009) Purification of cytoplasmic actin by affinity chromatography using the C-terminal half of gelsolin. Biochem Biophys Res Commun 383: 146–150.

50. Coulton A, Lehrer SS, Geeves MA (2006) Functional homodimers and heterodimers of recombinant smooth muscle tropomyosin. Biochemistry 45: 12853–12858.

51. Lehrer SS, Kerwar G (1972) Intrinsic fluorescence of actin. Biochemistry 11: 1211–1217.

52. Jochim N, Gerhard R, Just I, Pich A (2011) Impact of clostridial glucosylating toxins on the proteome of colonic cells determined by isotope-coded protein labeling and LC-MALDI. Proteome Sci 9: 48.

53. Müller M, Mazur AJ, Behrmann E, Diensthuber RP, Radke MB, et al. (2012) Functional characterization of the human alpha-cardiac actin mutations Y166C and M305L involved in hypertrophic cardiomyopathy. Cell Mol Life Sci.

54. Weiss S, Chizhov I, Geeves MA (2000) A flash photolysis fluorescence/light scattering apparatus for use with sub microgram quantities of muscle proteins. J Muscle Res Cell Motil 21: 423–432.

55. Anson M, Geeves MA, Kurzawa SE, Manstein DJ (1996) Myosin motors with artificial lever arms. EMBO J 15: 6069–6074.

56. Bookwalter CS, Trybus KM (2006) Functional consequences of a mutation in an expressed human alpha-cardiac actin at a site implicated in familial hypertrophic cardiomyopathy. J Biol Chem 281: 16777–16784.

57. Belyantseva IA, Perrin BJ, Sonnemann KJ, Zhu M, Stepanyan R, et al. (2009) Gamma-actin is required for cytoskeletal maintenance but not development. Proc Natl Acad Sci U S A 106: 9703–9708.

58. Choi BO, Hee Kang S, Hyun YS, Kanwal S, Park SW, et al. (2011) A complex phenotype of peripheral neuropathy, myopathy, hoarseness, and hearing loss is linked to an autosomal dominant mutation in MYH14. Hum Mutat 32: 669–677.

59. Bergeron SE, Zhu M, Thiem SM, Friderici KH, Rubenstein PA (2010) Ion-dependent polymerization differences between mammalian beta- and gamma-nonmuscle actin isoforms. J Biol Chem 285: 16087–16095.

60. Karakozova M, Kozak M, Wong CC, Bailey AO, Yates JR, 3rd, et al. (2006) Arginylation of beta-actin regulates actin cytoskeleton and cell motility. Science 313: 192–196.

61. Bryce NS, Schevzov G, Ferguson V, Percival JM, Lin JJ, et al. (2003) Specification of actin filament function and molecular composition by tropomyosin isoforms. Mol Biol Cell 14: 1002–1016.

62. Gunning P, O'Neill G, Hardeman E (2008) Tropomyosin-based regulation of the actin cytoskeleton in time and space. Physiol Rev 88: 1–35.